Interactive example 1 - Manuscript text

To study how the LRRK2 G2019S mutation impacts astrocytes in the prefrontal cortex, a cortical region linked to PD, we stained sections from the frontal cortices of age and sex-matched control and LRRK2 G2019S mutation-carrying PD patients with glial fibrillary acidic protein (GFAP, a marker for astrocyte branches) and phosphorylated ERM (Phospho-ERM, which are enriched in PAPs).

Interactive example 1 - Figure legend

Figure 1: ERM phosphorylation is impaired in PD patients carrying LRRK2 G2019S mutation. (A) Schematic of human frontal cortex regions analyzed for phospho-ERM staining. (B) Representative confocal images of GFAP (green) and phospho-ERM (purple) in the frontal cortex of human controls (n = 4; 3M, 1F) and LRRK2 G2019S mutation carriers (n = 3; 2M, 1F), aged > 80 years. Scale bar, 200 µm. (C) Quantification of GFA integrated density in (B). GFAP: t (5) = 2.822, p = 0.037; phospho-ERM: t (5) = 5.695, p = 0.0023. Grey dots: individual images; black dots: control averages; blue dots: mutation carrier averages.

Interactive example 1 Figure

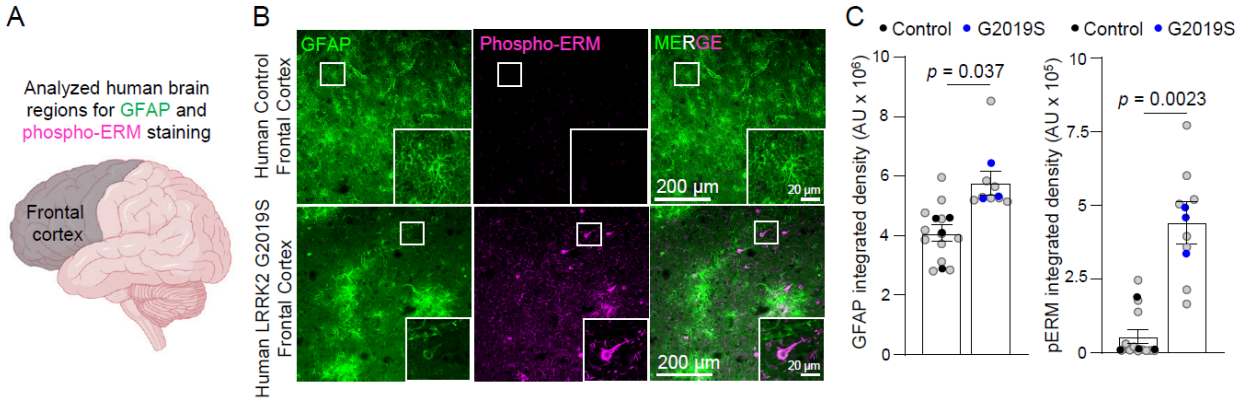

Interactive example 2- Manuscript text

Next, we used electrophysiology to assess how altered synapse density in the ACC and MOp of LRRK2 G2019Ski/ki mice affects synaptic function. We recorded miniature excitatory postsynaptic currents (mEPSCs) in the ACC L2-3 pyramidal neurons and miniature inhibitory postsynaptic currents (mIPSCs) in the MOp L2-3 pyramidal neurons from acute brain slices of P84 WT and LRRK2 G2019Ski/ki mice. LRRK2 G2019Ski/ki neurons displayed mEPSC frequency reduced by ~65% and a corresponding right shift in the cumulative distributions of mEPSC inter-event intervals (Figure 3A-B) when compared to WT neurons, with no change in mEPSC amplitude (Figure 3C).

Interactive example 2 - Figure legend

Figure 3: LRRK2 G2019S affects excitatory and inhibitory synapse function in the

ACC and MOp. (A) Representative mEPSC traces from ventral ACC L2-3 pyramidal neurons in WT and LRRK2 G2019Ski/ki mice. (B) Cumulative probability and quantification of mEPSC frequency: n = 15 (WT), 13 (LRRK2 G2019S ki/ki) neurons, 4 mice/genotype. Kolmogorov-Smirnov test: D = 0.504, p < 0.001. Mean frequency: WT (2.878 ± 0.6355), LRRK2 G2019S ki/ki (0.9673 ± 0.2328). Unpaired t-test: t (6) = 2.823, p = 0.0302.

Interactive example 2 - Figure

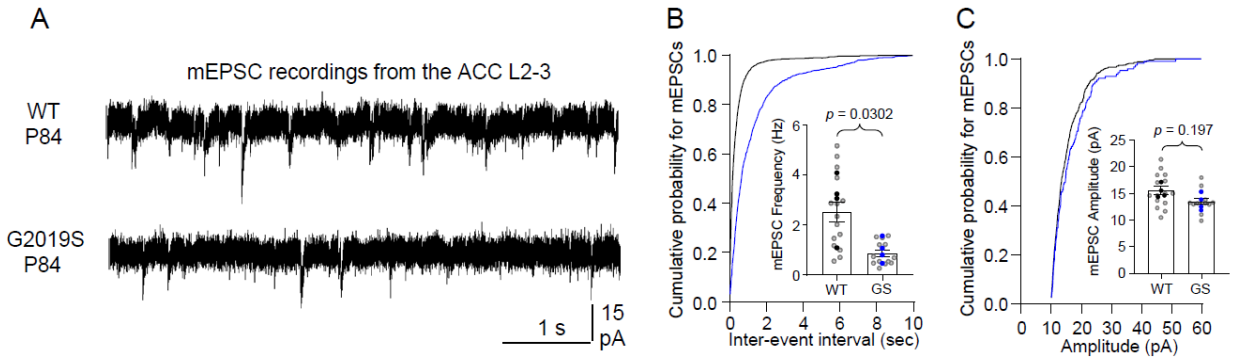

Interactive example 3 - Manuscript text

In vivo, Atg7 knockdown in WT astrocytes reduced astrocyte territory volume and morphological complexity, resembling the LRRK2 G2019Ski/ki astrocytes transfected with shControl (Figure 7I-K). In LRRK2 G2019S ki/ki astrocytes, Atg7 knockdown improved morphological complexity but did not further reduce territory volume (Figure 7J-K). These findings highlight Atg7's role in regulating astrocyte morphology and suggest its dysfunction in LRRK2 G2019Ski/ki astrocytes contributes to altered morphology.

Interactive example 3 - Figure legend

(I) Images of ACC and MOp L2-3 astrocytes at P21 expressing shControl or shAtg7-PB-mCherry-CAAX. Scale bar, 10 μm. (J) Quantification of astrocyte territories. Nested ANOVA [F(3,28) = 9.484, p = 0.0002] with Bonferroni tests: WT shControl vs. LRRK2 G2019Ski/ki shControl (p = 0.0036), WT shControl vs. WT shAtg7 (p = 0.0003), WT shAtg7 vs. LRRK2 G2019Ski/ki shAtg7 (p = 0.0109). n = 20–25 cells from 4–5 mice/group. (K) Astrocyte branching complexity. Two-way ANOVA revealed significant condition [F(2.324, 472.6) = 43.1, p < 0.05], radius [F(9, 250) = 301.8, p < 0.05], and interaction effects [F(27, 610) = 4.539, p < 0.05]. Bonferroni tests showed significant differences between groups, including WT shControl vs. LRRK2 G2019Ski/ki shControl (p < 0.0001) and WT shControl vs. WT shAtg7 (p < 0.0001).

Interactive example 3 - Figure

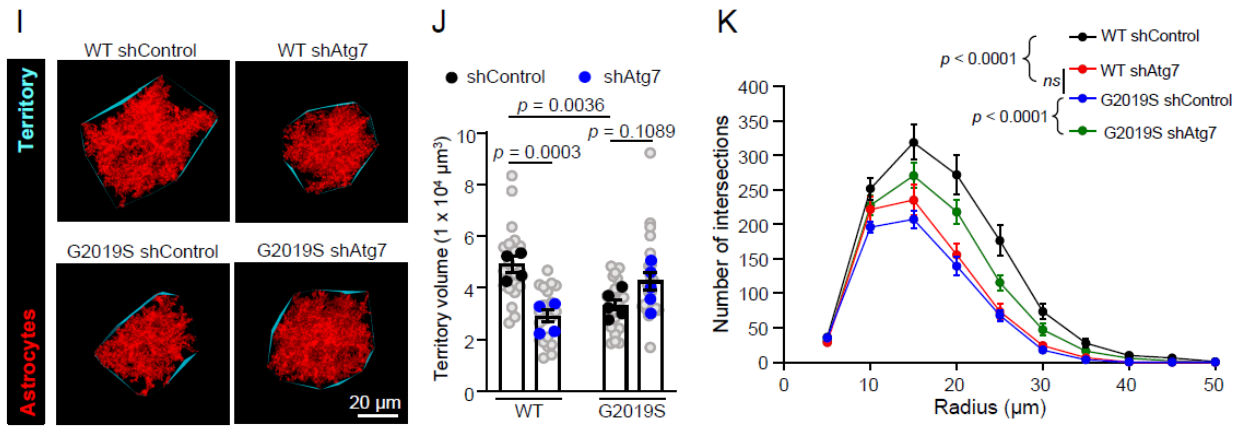
I
WT shControl
WT shAtg7
G2019S shControl
G2019S shAtg7
Territory
Astrocytes
20 µm
J
shControl
shAtg7
p = 0.0036
p = 0.1089
p = 0.0003
Territory volume (1 x 10⁴ µm³)
WT
G2019S
K
p < 0.0001
ns
p < 0.0001
WT shControl
WT shAtg7
G2019S shControl
G2019S shAtg7
Number of intersections
Radius (µm)